

First-principles study of crystal structures and superconductivity of ternary YSH₆ and LaSH₆ at high pressures

Xiaowei Liang,^{1,*} Shutao Zhao,^{1,2,*} Cancan Shao,^{1,*} Aitor Bergara,^{3,4,5} Hanyu Liu,⁶ Linyan Wang,¹ Rongxin Sun,¹ Yang Zhang,¹ Yufei Gao,¹ Zhisheng Zhao,¹ Xiang-Feng Zhou,¹ Julong He,¹ Dongli Yu,¹ Guoying Gao,^{1,†} and Yongjun Tian¹

¹Center for High Pressure Science, State Key Laboratory of Metastable Materials Science and Technology, Yanshan University, Qinhuangdao 066004, China

²School of Physics and Electronic Science, Fuyang Normal University, Fuyang 236037, China

³Departamento de Física de la Materia Condensada, Universidad del País Vasco, UPV/EHU, 48080 Bilbao, Spain

⁴Donostia International Physics Center (DIPC), 20018 Donostia, Spain

⁵Centro de Física de Materiales CFM, Centro Mixto CSIC-UPV/EHU, 20018 Donostia, Spain

⁶Innovation Center for Computational Physics Methods and Software & State Key Laboratory of Superhard Materials, College of Physics, Jilin University, Changchun 130012, China



(Received 29 June 2019; published 4 November 2019)

We have performed a systematic study on the crystal structures and electronic properties of two ternary hydrides, YSH₆ and LaSH₆, under pressure, using the particle swarm optimization method and first-principles calculations. As a result of extensive structure searches, metallic YSH₆ and LaSH₆ are thermodynamically stable between 195–237 and 170–300 GPa, respectively. Interestingly, in YSH₆ eight neighboring hydrogen atoms form octagons, and the octagons in different layers are connected by four sulfur atoms, forming a cagelike structure with a Y atom at the center, while those octagons in the same layer form polyphenylene-like chains via one shared side. In LaSH₆, however, hydrogen atoms form both curved “H₅” chains or straight chains when bonded to sulfur atoms. Furthermore, electron-phonon coupling calculations indicate that YSH₆ and LaSH₆ are promising superconductors with estimated T_c values of 91 and 35 K at 210 and 300 GPa, respectively. These results provide guidance for future experimental studies and stimulate more exploration on ternary hydrides.

DOI: [10.1103/PhysRevB.100.184502](https://doi.org/10.1103/PhysRevB.100.184502)

I. INTRODUCTION

The search for high critical (T_c) or even room-temperature superconductors remains one of the most exciting research topics and has attracted great interest because of their fundamental and practical applications. Since Ashcroft [1] suggested that hydrogen-rich materials might be potential high- T_c superconductors at lower pressures than that of solid hydrogen due to “precompressing effects,” much experimental and theoretical effort has been devoted to the investigation of many hydrides with high T_c [2–28]. Encouragingly, hydrides formed by some elements in the chalcogen, alkaline earth, or rare-earth groups have recently been reported to have T_c values over 200 K [3–11,13–15]. Compressed H₂S was predicted to have a T_c of 80 K above 100 GPa [2], which was later confirmed experimentally [4]. Moreover, another “high-temperature sample” was also obtained with a higher T_c of 203 K at 150 GPa, in agreement with a previous theoretical prediction [3]. CaH₆, YH₆, MgH₆, and recently predicted ternary CaYH₁₂, all with hydrogen clathrate frameworks, were predicted to exhibit even higher T_c values at high pressure [6–9]. The rare-earth hydrides, YH₁₀ and LaH₁₀, were predicted to be stable in a $Fm\bar{3}m$ structure with H₃₂ cages and

estimated to be superconductors with T_c values over 280 K [10,11]. These predictions have been recently confirmed, as $Fm\bar{3}m$ LaH₁₀ was successfully synthesized at 170 GPa on heating to about 1000 K [12], and multiple measurements revealed its high T_c values of 250–260 K at 170–190 GPa [13,14].

Such achievements enhanced the interest in further searching possible room-temperature superconducting hydrides, and ternary hydrogen-rich compounds are interesting candidates. BaReH₉ was reported experimentally to be a superconductor under pressure, with a T_c of about 7 K above 100 GPa [22]. Ba(AuH₂)₂ and Sr(AuH₂)₂ were predicted to be superconductors below 30 and 10 K at 1 atm, respectively [23]. $Cmc2_1$ Fe₂SH₃, $Fm\bar{3}m$ Li₂BH₆, and $Pm\bar{3}$ MgSiH₆ and MgGeH₆ were reported to have T_c values of 0.3, 100, 63, and 67 K at 173, 100, 250, and 200 GPa, respectively [24–27]. Moreover, three phases of H₆SSe, similar to $Im\bar{3}m$ H₃S, were predicted to be superconductors with T_c decreasing from 195 to 115 K as the strength of the weakest covalent H-S or H-Se bonds in these structures declines [28]. In addition, our recent work on CaYH₁₂ showed that its estimated T_c might reach 258 K at 200 GPa [9], which encouraged us to search for high- T_c superconductors in other ternary hydrides.

In this paper, high-pressure structures and superconductivity of YSH₆ and LaSH₆ were investigated by a combination of the particle swarm optimization algorithm and first-principles calculations. Under pressure, rare-earth elements are expected

*These authors contributed equally to this work.

†gaoguoying@ysu.edu.cn

to transfer electrons to hydrogen atoms occupying their antibonding orbitals, which might induce the decomposition of H_2 dimers [29] and help the formation of hydrides [7–11]. Meanwhile, S atoms might form covalent bonds with Hs, preventing the formation of H_2 molecules, which might play a critical role in the superconducting transition [3,28]. Interestingly, new cage-like frameworks containing two octagons and four S atoms were predicted to be stable in YSH_6 with $P4_2/mmc$ symmetry. In addition, curved “ H_5 ” and straight “ $H-S$ ” chains were revealed in the $Cmcm$ phase of $LaSH_6$. Electron-phonon coupling (EPC) calculations suggested that both phases are promising candidates as superconducting materials.

II. COMPUTATIONAL DETAILS

To obtain the stable structures of ternary hydrides YSH_6 and $LaSH_6$ at high pressures, we conducted structure predictions based on the particle swarm optimization algorithm as implemented in the CALYPSO package [30,31]. This method has been applied successfully to many crystalline systems ranging from elemental solids to binary and ternary compounds and has been proven to be a powerful tool for predicting high-pressure structures [2,32,33]. The structural relaxation and electronic structure calculations were performed in the framework of density functional theory using the Perdew-Burke-Ernzerhof generalized gradient approximation method [34] as implemented in the Vienna ab initio simulation package code [35]. The frozen-core all-electron projector-augmented wave method was used, where $4s^2 4p^6 4d^1 5s^2$, $5s^2 5p^6 5d^1 6s^2$, $3s^2 3p^4$, and $1s^1$ are treated as valence electrons for Y, La, S, and H, respectively. A plane wave cutoff energy of 600 eV and appropriate Monkhorst-Pack [36] k -meshes were tested and converged to less than 1 meV/atom. Phonon dispersion and EPC calculations were performed within the density functional perturbation theory, as implemented in the QUANTUM ESPRESSO package [37], where norm-conserving pseudopotentials for Y, La, S, and H were considered with a kinetic energy cutoff of 80 Ry. $8 \times 8 \times 3$ and $8 \times 8 \times 4$ q -meshes in the first Brillouin zones were used in the EPC calculations for $P4_2/mmc$ YSH_6 and $Cmcm$ $LaSH_6$, respectively.

III. RESULTS AND DISCUSSION

Here crystal structural predictions were performed at pressures of 50, 100, 200, and 300 GPa, with unit cells containing up to four formula units. For YSH_6 , three new phases, Cm , $P1$, and $C2/m$, were predicted below 200 GPa with H atoms both in the form of “ H_2 ” units and monatomic H (Fig. S1 [38]). However, with increasing pressure, a tetragonal $P4_2/mmc$ structure becomes the preferred one, and H atoms evolve from “ H_2 ” units in low-pressure structures to “ H_8 ” octagons in high-pressure $P4_2/mmc$ [Fig. 1(a)]. There are three types of H-H bonds in the octagon, with distances of 0.893 Å (H1-H2), 0.934 Å (H3-H4), and 1.254 Å (H2-H3) at 200 GPa. The shortest H-H bond length (0.893 Å) is longer than that of 0.743 Å in pure H_2 solid at the same pressure [39]. The longest hydrogen bond of 1.254 Å is close to that in YH_6 (1.241 Å) at 200 GPa [7], indicating the existence of weak covalent

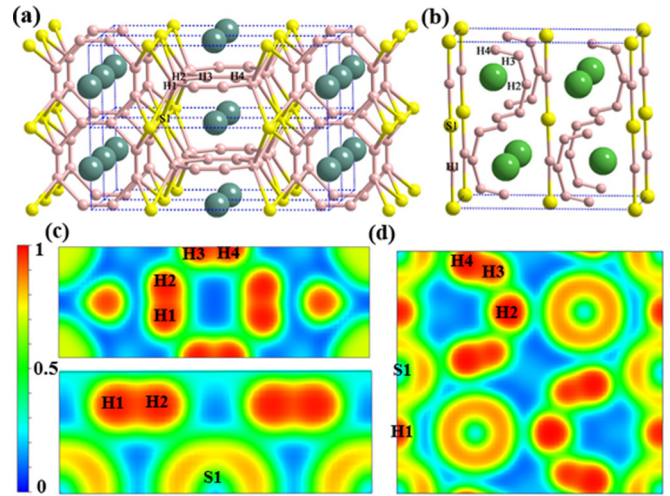


FIG. 1. Predicted crystal structures of (a) $P4_2/mmc$ YSH_6 and (b) $Cmcm$ $LaSH_6$ at 200 GPa. The Y (dark green), La (green), S (yellow), and H (pink) atoms are represented by the colored spheres. The lower panel shows the electronic localization function of (c) $P4_2/mmc$ YSH_6 and (d) $Cmcm$ $LaSH_6$ at 200 GPa.

interactions. As pressure increases to 300 GPa, the nearest and second-nearest bond lengths in the octagon increase to 0.919 and 0.956 Å, respectively, while the longest one becomes shorter (1.179 Å). Pressure is a useful tool to help the dissociation of H_2 dimers, making H octagons more regular and stable. Moreover, H octagons in different layers are connected with each other by four S atoms, building a cage-like structure with a Y atom at the center, while those octagons in the same layer share one side and form polyphenylene-like chains.

For $LaSH_6$, three phases, $P1$, $P\bar{1}$, and $Cmcm$, were predicted at different pressures by means of extensive structure searches. As in YSH_6 , the lower-pressure $P1$ and $P\bar{1}$ structures of $LaSH_6$ (Fig. S1 [38]) show monoatomic H combined with H_2 and H_3 units. In the higher-pressure $Cmcm$ phase [Fig. 1(b)], some hydrogen atoms form curved “ H_5 ” chains, which is different from the octagonal character presented in $P4_2/mmc$ YSH_6 . “ H_5 ” chains and La atoms are arranged alternately along the coordinate axis and present two kinds of H-H bonds, with 0.856 (H3-H4) and 1.128 Å (H2-H3) lengths. The H-H bond length of 1.128 Å is close to that of 1.109–1.196 Å in LaH_{10} at 200 GPa [10,11]. The remaining H atoms are bonded with S atoms and form straight chains, which are parallel to each other along the coordinate axis. The length of the H-S bond is 1.60 Å, which is longer than that in $Im\bar{3}m$ H_3S (1.492 Å) [3]. Moreover, the trend of H-H distances in the “ H_5 ” chain with pressure is also similar to those found in the octagon in $P4_2/mmc$ YSH_6 . The smallest bond length becomes longer (0.88 Å at 300 GPa), while the longest one becomes shorter (1.09 Å at 300 GPa).

The calculated relative enthalpy curves for the predicted structures of YSH_6 and $LaSH_6$ as a function of pressure are presented in Fig. 2. On the basis of corresponding binary compounds, the decomposition enthalpies into $YS(LaS) + 3H_2$, $Y(La)H_3 + H_3S$, $Y(La)H_4 + H_2S$, and $Y(La)H_6 + S$ are considered in order to investigate the phase stability of YSH_6 and $LaSH_6$ at high pressures.

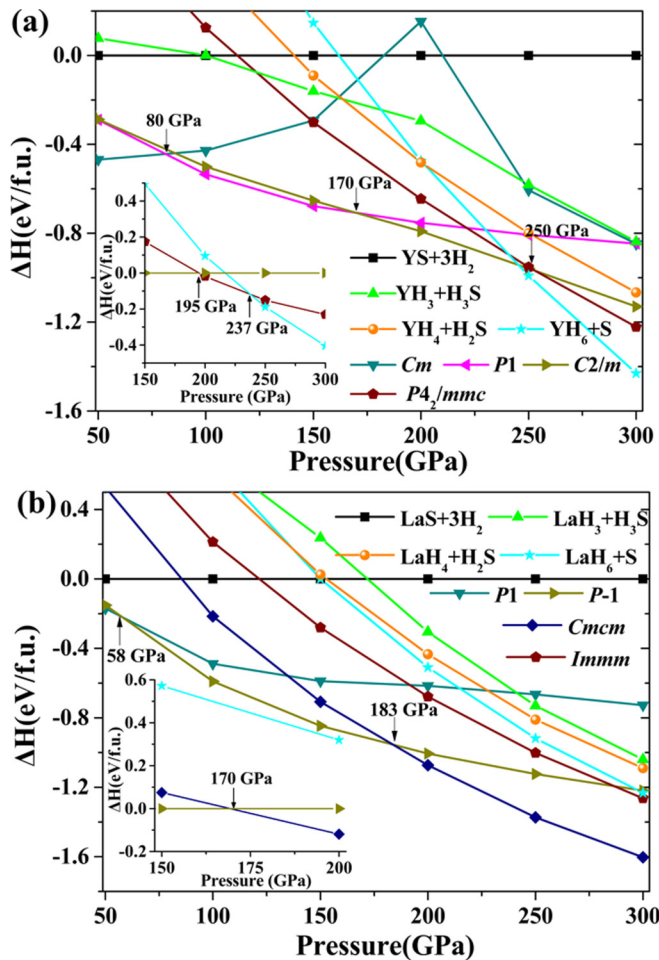


FIG. 2. Enthalpy curves per formula unit as a function of pressure for (a) YSH_6 and (b) LaSH_6 with respect to $3\text{H}_2 + \text{YS}$ and $3\text{H}_2 + \text{LaS}$. The decomposition enthalpies for Y(La)SH_6 to $\text{Y(La)H}_3 + \text{H}_3\text{S}$, $\text{Y(La)H}_4 + \text{H}_2\text{S}$, and $\text{Y(La)H}_6 + \text{S}$ are also presented. The most stable structure at the corresponding pressure for each stoichiometry is considered [3,7,11,39,40]. The enthalpies of some structures for Y(La)SH_6 as a function of pressure including zero-point corrections are shown in the insets.

As shown in Fig. 2(a), YSH_6 emerges in a Cm structure at 50 GPa and then transforms to $P1$ and $C2/m$ structures at 80 and 170 GPa, respectively. Above 250 GPa, the $P4_2/mmc$ structure is predicted to be energetically preferred. However, it was metastable with higher enthalpies relative to YH_6 and S decomposition. Considering that, due to the low mass of hydrogen, including zero-point energy (ZPE) contributions might be essential in determining the structural stability of hydrogen-rich compounds [39]. ZPE corrections for the predicted $C2/m$ and $P4_2/mmc$ YSH_6 , as well as for YH_6 and S , were calculated within the quasiharmonic approximation at 150, 200, 250, and 300 GPa [41]. As shown in the inset of Fig. 2(a), with considering ZPE contributions, the transition pressure from $C2/m$ to $P4_2/mmc$ decreases from 250 to 195 GPa, and the $P4_2/mmc$ phase becomes stable with respect to YH_6 and S decomposition between 195 and 237 GPa.

For LaSH_6 , the phase transition from $P1$ to $P\bar{1}$ structure occurs at 58 GPa. $P\bar{1}$ and $Cmcm$ structures become the most stable phases between 58–183 and 183–300 GPa, respectively

[Fig. 2(b)]. Including the ZPEs contribution, the predicted $P\bar{1}$ and $Cmcm$ structures are still stable with respect to decomposition. Moreover, the stabilization pressure of the $Cmcm$ structure also decreases from 183 to 170 GPa.

In order to explore the bonding information, the electronic localization function (ELF) [42,43] of $P4_2/mmc$ YSH_6 and $Cmcm$ LaSH_6 were calculated at 200 GPa. The ELF slice for $P4_2/mmc$ YSH_6 containing the hydrogen octagon is shown at the top panel of Fig. 1(c), the ELF values for the H1-H2 and H3-H4 bonds are larger than 0.9, indicating that they are strong covalent bonds. The ELF value at the center of the H2-H3 bond in the octagon is approximately 0.5, which is the corresponding value for the homogeneous electron gas. From the lower panel, we can conclude there is a weak interaction between S and H1 (H2) atoms. Similarly, for $Cmcm$ LaSH_6 [Fig. 1(d)], the very large ELF value at the H3-H4 bond (close to 1) and a smaller one at the H2-H3 bond (around 0.6) indicate their covalent characters, as well as the expected S1-H1 covalent bond with an ELF of about 0.7.

Electronic topological analysis was subsequently performed to further investigate their chemical bonding [44]. In $P4_2/mmc$ YSH_6 , there are electron charge transfers from Y to H and S atoms. Each H_2 accepts 0.18 electrons on average, as transferred from Y atoms, which occupy their antibonding orbitals, elongating the H-H bond length [6,45]. In addition, H_2 intermolecular distances decrease on compression and stretched H_2 dimers tend to form octagons under pressure. Compared with rare-earth hydrides with clathrate structures [7,10], in $P4_2/mmc$ YSH_6 , S atoms attract some electrons donated by Y s. Besides, the H content in YSH_6 is relatively lower compared with rare-earth hydrides. Thus, in YSH_6 there are H octagons rather than denser clathrate structures. For $Cmcm$ LaSH_6 , La and S atoms act as electron donors and acceptors, respectively. According to our calculations, most of the H atoms accept electrons, except for those in the middle of curved H_5 chains, which donate electrons.

In order to investigate the phase stability mechanism of $P4_2/mmc$ YSH_6 and $Cmcm$ LaSH_6 , we have calculated the internal energies (U) and the product of pressure and volume (PV) contributions to the enthalpy relative to $\text{YH}_6 + \text{S}$ and $\text{LaH}_6 + \text{S}$, respectively (Fig. S2 [38]). According to our calculations, the PV terms of Y(La)SH_6 are always higher than those of $\text{Y(La)H}_6 + \text{S}$, while the U terms show the opposite trend, so that negative ΔU terms are mainly responsible for the overall negative relative enthalpy under pressure. These results indicate that diverse H-S, Y(La)-S , and H-H bonds in Y(La)SH_6 may be the key driving mechanism for its phase stability.

With the aim to search for metallic and superconducting materials, we explored the electronic band structures for the predicted phases of YSH_6 and LaSH_6 . For YSH_6 , the Cm , $P1$, and $C2/m$ structures were calculated to be semiconductors with indirect band gaps of 2.54, 1.12, and 0.14 eV at 50, 100, and 200 GPa, respectively (Fig. S3 [38]). The bands for Cm and $P1$ phases are quite flat at lower pressures, associated with their strong electronic localization. Similarly, $P\bar{1}$ LaSH_6 (Fig. S3d [38]) is also a semiconductor with an indirect band gap of 1.56 eV at 50 GPa. Upon compression, $P\bar{1}$ LaSH_6 becomes a metal at 150 GPa. Additionally, both high-pressure $P4_2/mmc$ YSH_6 and $Cmcm$ LaSH_6 are good metals at 210 and 200 GPa,

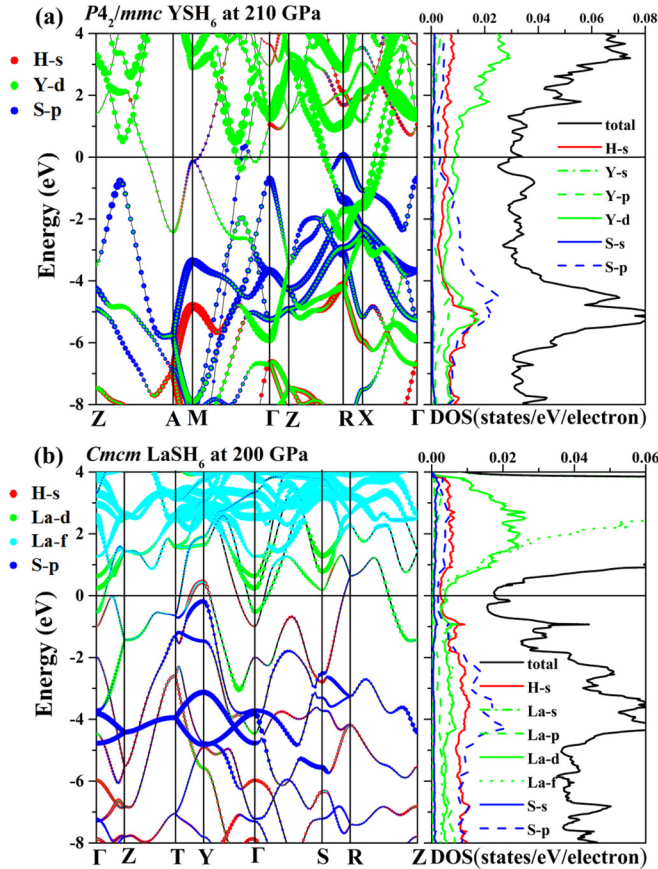


FIG. 3. The calculated band structures and DOS of the predicted crystal structures (a) $P4_2/mmc$ YSH_6 and (b) Cmc $LaSH_6$ at 210 and 200 GPa. The bands projected onto Yd ($La d$ and f), Sp , and HS orbitals are displayed in the band structures (the radii of the circles are proportional to the weights of the corresponding orbitals).

respectively, with several bands crossing the Fermi level (E_f) (Fig. 3). Band projections onto Yd ($La d$ and f), Sp , and HS orbitals are also shown in both band structures. These orbitals are the main contributions to the electronic states near the E_f , which mainly contribute to the electron-phonon coupling. In addition to some steep bands crossing the E_f , some holelike and electron-like bands are also found near the E_f (around M and R points for YSH_6 ; Y , Γ points and along the Γ - Z direction for $LaSH_6$), giving rise to a large density of states (DOS) (Fig. 3 and Fig. S4 [38]), which enhances the electron-phonon coupling strength [46–51].

The dynamical stabilities of $P4_2/mmc$ YSH_6 and Cmc $LaSH_6$ were investigated by calculating their phonon dispersion curves. As shown in Fig. 4, the absence of any imaginary frequency confirms their dynamical stability at 210 and 200 GPa, respectively. Significant phonon softening can be seen in phonon branches along Z - A - M - Γ and R - X directions for $P4_2/mmc$ YSH_6 and Γ - S - R direction for Cmc $LaSH_6$. These soft modes are mainly associated with vibrations of H atoms (Figs. S5 and S6 [38]). Moreover, phonon softenings of H branches are associated with large contributions to λ and high T_c values as known in some high- T_c hydrides [3, 7, 10, 11]. To explore potential superconductivity of ternary hydrides $P4_2/mmc$ YSH_6 and Cmc $LaSH_6$, we have also studied their projected phonon DOS, the EPC parameter λ ,

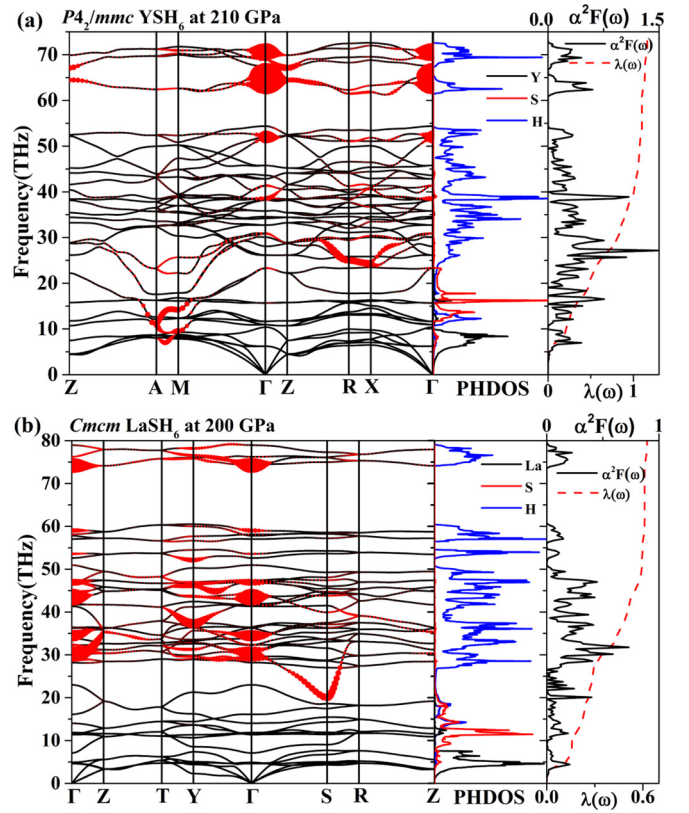


FIG. 4. Phonon dispersion curves (the radius of the red circles is proportional to the phonon linewidth), phonon density of states, Eliashberg phonon spectral function $\alpha^2F(\omega)$ and the integrated λ of the predicted crystal structures (a) $P4_2/mmc$ YSH_6 at 210 GPa and (b) Cmc $LaSH_6$ at 200 GPa.

and the Eliashberg phonon spectral function $\alpha^2F(\omega)$ at 210 and 200 GPa (Fig. 4), respectively. As shown in the projected phonon DOS, the vibrations of the heavier Y and La atoms in $P4_2/mmc$ YSH_6 and Cmc $LaSH_6$ are associated with the low-frequency phonon branches, while vibrations of S and H atoms are mainly related to the middle- and high-frequency regions, respectively. For $P4_2/mmc$ YSH_6 , the two main ingredients to estimate T_c ($T_c = \frac{\omega_{\log}}{1.2} \exp[-\frac{1.04(1+\lambda)}{\lambda - \mu^*(1+0.62\lambda)}]$) [52], the logarithmic average frequency, ω_{\log} , and the EPC parameters, λ , are calculated to be 1048 K and 1.17, respectively. The origin of λ can be understood by analyzing the Eliashberg phonon spectral function, $\alpha^2F(\omega)$. As shown in the right panel of Fig. 4(a), the spectrum of $\alpha^2F(\omega)$ is roughly proportional to the phonon DOS between 30 and 55 THz, dominated by H modes. Between 20 and 30 THz, the values of phonon DOS are relatively low, but pronounced peaks appear in the $\alpha^2F(\omega)$ curves, which show the strong coupling strength from phonons in this frequency range. To further explore the contributions of different phonon modes, red circles with the radius proportional to the phonon linewidth are also plotted in the first panel of Fig. 4(a). The high-frequency modes (above 60 THz) at the Γ point and the soft modes along Z - R - X - Γ (between 20 and 30 THz) and A - M (between 5 and 15 THz) directions show quite large phonon linewidths, enhancing the EPC parameter. At 300 GPa, the calculated ω_{\log} increases to 1437 K, while λ decreases to 0.76 (Fig. 5). It is seen that

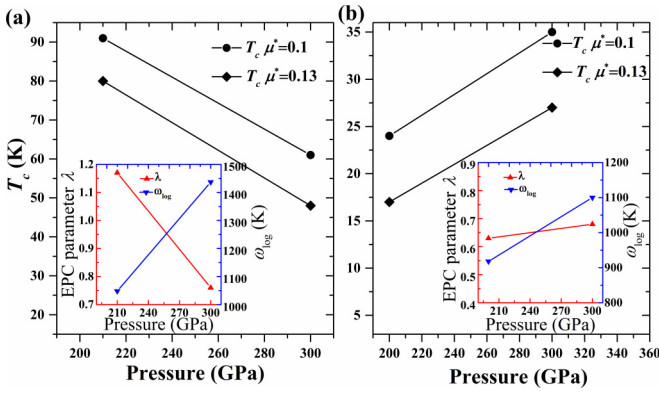


FIG. 5. The calculated T_c values as a function of pressure for (a) $P4_2/mmc$ YSH₆ and (b) $Cmcm$ LaSH₆. The insets show the EPC parameter λ and logarithmic average frequency ω_{\log} as a function of pressure.

the peaks of $\alpha^2F(\omega)$ are mainly associated to H vibrations (Fig. S7 [38]), which play a critical role in the EPC, with a 75% contribution to the total λ . Phonon modes become stiffer with pressure and, therefore, ω_{\log} increases. Moreover, $\alpha^2F(\omega)$ at 300 GPa is almost simply shifted to a high-frequency region (Fig. S7 [38]), which weakens $\alpha^2F(\omega)/\omega$ due to the increase of ω , and thus λ [$\lambda = 2 \int_0^\infty \alpha^2F(\omega)/\omega d\omega$] decreases with pressure.

For $Cmcm$ LaSH₆ [Fig. 4(b)], vibrations of H atoms above 20 THz contribute 56% of the total λ of 0.63, whereas the remaining 44% comes from vibrations of other Hs, La, and S atoms. As shown in the $\alpha^2F(\omega)$ curves, the main peaks emerge between 30 and 50 THz. In this frequency range some modes around Γ and Y points give important contributions to λ , which is different from $P4_2/mmc$ YSH₆, where the main peaks show up at the frequency region of the soft modes. Comparing the phonon spectra of $P4_2/mmc$ YSH₆ with $Cmcm$ LaSH₆, there are many soft modes in $P4_2/mmc$ YSH₆, while only one along the Γ - S - R direction between 20 and 30 THz in $Cmcm$ LaSH₆. Although this soft mode also enhances λ , the vibrations between 30 and 50 THz still remain dominant. As pressure increases to 300 GPa, ω_{\log} increases from 918 to 1100 K (Fig. 5). Although phonon modes also become stiffer with pressure, $\alpha^2F(\omega)$ generally increases with pressure and the calculated total λ rises a little, from 0.63 to 0.68 (Fig. 5). At 300 GPa the main contribution to λ corresponds to H vibrations (63%) (Fig. S7 [38]), so that H-associated phonons are mainly responsible for the EPC parameter λ in the Y(La)SH₆. This indicates that a large number of electronic states [Y d (La d and f), S p , and H s for Y(La)SH₆] at the E_f are coupled to the H-derived phonon modes, therefore enhancing the superconducting transition.

Superconducting transition temperatures of $P4_2/mmc$ YSH₆ and $Cmcm$ LaSH₆ are evaluated through the Allen-Dynes modified McMillan equation [52]. The estimated T_c values for the $P4_2/mmc$ YSH₆ and $Cmcm$ LaSH₆ at 210 and 200 GPa are 80–91 and 17–24 K, respectively, using Coulomb pseudopotential parameter μ^* of 0.13 and 0.1. As shown in Fig. 5, the trend of T_c as a function of pressure was also investigated for both structures. As pressure increases from 210 to 300 GPa, the estimated T_c for $P4_2/mmc$ YSH₆

decreases from 91 to 61 K with μ^* of 0.1, which follows the trend of λ with pressure. T_c reaches a maximum at the pressure in which the crystal structure becomes dynamically unstable, which is similar to some other high- T_c hydrides [10,11]. On the other hand, for $Cmcm$ LaSH₆ both ω_{\log} and λ increase with pressure, and therefore the calculated T_c also rises from 24 to 35 K. Moreover, we have also investigated the constituent atomic contributions (non-H atoms and H) to T_c at 300 GPa (Table S1 [38]). Similar to other hydrides [53,54], H atoms have positive effects on increasing both λ and ω_{\log} , determining T_c . On the other hand, although non-H atoms also increase the total λ , they decrease ω_{\log} . Our results reveal that the positive effect on T_c of λ associated with non-H atoms overcomes the negative effect of ω_{\log} in both $P4_2/mmc$ YSH₆ and $Cmcm$ LaSH₆.

As is well known, the corresponding binary hydrides of YSH₆ and LaSH₆, such as H₃S, YH₆, YH₁₀, and LaH₁₀, have been observed or estimated to be excellent superconductors, with T_c s over 200 K under pressure. In comparison, YSH₆ and LaSH₆ have lower T_c s, mainly due to their smaller EPC parameter λ (Table I). According to the simplified Hopfield expression, $\lambda = \frac{N(E_f)\langle I^2 \rangle}{M\langle \omega^2 \rangle}$ [55], where $N(E_f)$ is the calculated electronic DOS at Fermi level, $\langle I^2 \rangle$ is the average over the Fermi surface of the square of the electron-ion matrix element, M is the ion mass, and $\langle \omega^2 \rangle$ is the average of the square phonon frequencies, which could be derived from the spectral function $\alpha^2F(\omega)$ [56]. λ is roughly proportional to the $N(E_f)$ and, therefore, a large $N(E_f)$ might enhance λ . As shown in Fig. S4 [38], the $N(E_f)$ of $P4_2/mmc$ YSH₆ is comparable to that of those hydrides with strong EPC, while it is slightly smaller for $Cmcm$ LaSH₆. Meanwhile, the values of $\langle \omega^2 \rangle$ (Table I) are smaller overall for $P4_2/mmc$ YSH₆ and $Cmcm$ LaSH₆ at 210 and 200 GPa. Therefore, the smaller impact of the displacement of the atoms on the electronic structure, as well as the heavier atomic mass resulting from the lower H contents of $P4_2/mmc$ YSH₆ and $Cmcm$ LaSH₆ become mainly responsible for their lower λ and T_c values. Previous studies show that hydrogenic sublattices in hydrides are important to get high T_c values [18,46–48]. However, the presence of isolated hydrogenic motifs (H⁻ or H₂) might not imply a high T_c , but hydrides containing clathrate H lattices, such as YH₁₀ and LaH₁₀, show remarkably high T_c s. In addition, rare-earth hydrides with one- or two-dimensional hydrogenic lattices (ScH₉, ScH₁₀, ScH₁₂, and LaH₈) are also usually estimated to have T_c values intermediate to the other two classes of systems described above [18]. Interestingly, in $C2/m$ LaH₈ [11] we found traces of curved H₅ units similar to those in $Cmcm$ LaSH₆. As they have more H atoms, curved H₅ units are linked by other H atoms and form two-dimensional hydrogenic lattices with edge-sharing puckered dodecagons in $C2/m$ LaH₈, while there are curved H₅ chains in $Cmcm$ LaSH₆. Thus, the estimated λ in $Cmcm$ LaSH₆ at 200 GPa (0.63) is smaller than in $C2/m$ LaH₈ at 300 GPa (1.12), and considering that ω_{\log} is also smaller, it results in a lower T_c . In $P4_2/mmc$ YSH₆, the H octagons sharing one edge form extended one-dimensional structures, similar to $C2/m$ LaH₈. The calculated λ in $P4_2/mmc$ YSH₆ at 200 GPa (1.17) is close to the values in $C2/m$ LaH₈ at 300 GPa (1.12), $Cmcm$ ScH₁₀ at 250 GPa (1.17), and $Immm$ ScH₁₂ at 350 GPa (1.17).

TABLE I. The calculated EPC parameter λ , square root of the average square phonon frequencies $\langle\omega^2\rangle^{1/2}$, logarithmic average frequency ω_{\log} , and critical temperature T_c with μ^* of 0.1 for $P4_2/mmc$ YSH₆, $Cmcm$ LaSH₆, $Im\bar{3}m$ H₃S, $Im\bar{3}m$ YH₆, $Fm\bar{3}m$ YH₁₀, and LaH₁₀ at different pressures.

	P (GPa)	λ	$\langle\omega^2\rangle^{1/2}$ (K)	ω_{\log} (K)	T_c with $\mu^* = 0.1$ (K)
$P4_2/mmc$ -YSH ₆	210	1.17	1428	1048	91
$P4_2/mmc$ -YSH ₆	300	0.76	1770	1437	61
$Cmcm$ -LaSH ₆	200	0.63	1493	918	24
$Cmcm$ -LaSH ₆	300	0.68	1739	1100	35
$Im\bar{3}m$ -H ₃ S	200	1.95	1551	1349	191, 223 ^a
$Im\bar{3}m$ -YH ₆ ^b	200	1.88	1666	1283	177, 209 ^a
$Fm\bar{3}m$ -YH ₁₀	300	2.06 ^c	1564 ^c	1511 ^c	255 ^{a,c}
		2.42 ^d	1751 ^d	1311 ^d	271 ^{a,d}
$Fm\bar{3}m$ -LaH ₁₀	250	2.29 ^c	1325 ^c	1253 ^c	232 ^{a,c}
		2.46 ^d	1415 ^d	1067 ^d	223 ^{a,d}

^aThe calculated T_c values are based on the McMillan equation with the strong-coupling and the shape corrections; ^bRef. [9]; ^cRef. [11]; ^dRef. [54].

However, the calculated T_c of $P4_2/mmc$ YSH₆ (91 K) is lower than others due to the smaller ω_{\log} , which can be related to its different H content.

IV. CONCLUSIONS

In summary, we have systematically analyzed crystal structures and electronic properties of ternary hydrides YSH₆ and LaSH₆ under pressure. In YSH₆, a $P4_2/mmc$ structure is predicted to be stable with pressure and it contains cagelike structures formed by hydrogen octagons connected by sulfur atoms with a Y atom at the center, which is different from the predicted stable phases at low pressure with monoatomic H and H₂ units. Similarly, a unique $Cmcm$ structure for LaSH₆ is predicted to be stable under pressure with curved “H₅” and straight “H-S” chains. The calculated electronic band structures show the metallic feature of both $P4_2/mmc$ YSH₆ and $Cmcm$ LaSH₆. Further electron-phonon coupling calculations indicate that both structures become potential superconductors with estimated T_c values of 91 and 35 K at 210

and 300 GPa, respectively, suggesting that cagelike structures favor a high T_c . These results might further stimulate future experimental synthesis and more theoretical studies on ternary hydrides.

ACKNOWLEDGMENTS

The work was supported by the National Natural Science Foundation of China (Grants No. 11604290 and No. 51732010), National Key R & D Program of China (Grant No. 2018YFA0703400), Funding Program for Recruited Oversea Scholars of Hebei Province (Grant No. CL201729), the Ph.D. Foundation by Yanshan University (Grant No. B970), and the Natural Science Research Project of Education Department of Anhui Province (KJ2018A0342). A.B. acknowledges financial support from the Spanish Ministry of Economy and Competitiveness (FIS2016-76617-P) and the Department of Education, Universities and Research of the Basque Government and the University of the Basque Country (IT756-13).

- [1] N. W. Ashcroft, *Phys. Rev. Lett.* **92**, 187002 (2004).
- [2] Y. Li, J. Hao, H. Liu, Y. Li, and Y. Ma, *J. Chem. Phys.* **140**, 174712 (2014).
- [3] D. Duan, Y. Liu, F. Tian, D. Li, X. Huang, Z. Zhao, H. Yu, B. Liu, W. Tian, and T. Cui, *Sci. Rep.* **4**, 6968 (2014).
- [4] A. P. Drozdov, M. I. Eremets, I. A. Troyan, V. Ksenofontov, and S. I. Shylin, *Nature* **525**, 73 (2015).
- [5] M. Einaga, M. Sakata, T. Ishikawa, K. Shimizu, M. Eremets, A. Drozdov, I. Troyan, N. Hirao, and Y. Ohishi, *Nat. Phys.* **12**, 835 (2016).
- [6] H. Wang, J. S. Tse, K. Tanaka, T. Iitaka, and Y. Ma, *Proc. Natl. Acad. Sci. USA* **109**, 6463 (2012).
- [7] Y. Li, J. Hao, H. Liu, J. Tse, Y. Wang, and Y. Ma, *Sci. Rep.* **5**, 9948 (2015).
- [8] X. Feng, J. Zhang, G. Gao, H. Liu, and H. Wang, *RSC Adv.* **5**, 59292 (2015).
- [9] X. Liang, A. Bergara, L. Wang, B. Wen, Z. Zhao, X.-F. Zhou, J. He, G. Gao, and Y. Tian, *Phys. Rev. B* **99**, 100505(R) (2019).
- [10] F. Peng, Y. Sun, C. J. Pickard, R. J. Needs, Q. Wu, and Y. Ma, *Phys. Rev. Lett.* **119**, 107001 (2017).
- [11] H. Liu, I. I. Naumov, R. Hoffmann, N. W. Ashcroft, and R. J. Hemley, *Proc. Natl. Acad. Sci. USA* **114**, 6990 (2017).
- [12] Z. M. Geballe, H. Liu, A. K. Mishra, M. Ahart, M. Somayazulu, Y. Meng, M. Baldini, and R. J. Hemley, *Angew. Chem. Int. Ed.* **57**, 688 (2018).
- [13] M. Somayazulu, M. Ahart, A. K. Mishra, Z. M. Geballe, M. Baldini, Y. Meng, V. V. Struzhkin, and R. J. Hemley, *Phys. Rev. Lett.* **122**, 027001 (2019).
- [14] A. Drozdov, P. Kong, V. Minkov, S. Besedin, M. Kuzovnikov, S. Mozaffari, L. Balicas, F. Balakirev, D. Graf, V. Prakapenka *et al.*, *Nature* **569**, 528 (2019).
- [15] A. G. Kvashnin, D. V. Semenov, I. A. Kruglov, I. A. Wrona, and A. R. Oganov, *ACS Appl. Mater. Int.* **10**, 43809 (2018).
- [16] I. A. Kruglov, A. G. Kvashnin, A. F. Goncharov, A. R. Oganov, S. S. Lobanov, N. Holtgrewe, S. Jiang, V. B. Prakapenka, E. Greenberg, and A. V. Yanilkin, *Sci. Adv.* **4**, eaat9776 (2018).

- [17] D. V. Semenok, I. A. Kruglov, A. G. Kvashnin, and A. R. Oganov, [arXiv:1806.00865](https://arxiv.org/abs/1806.00865).
- [18] E. Zurek and T. Bi, *J Chem. Phys.* **150**, 050901 (2019).
- [19] G. Gao, H. Wang, A. Bergara, Y. Li, G. Liu, and Y. Ma, *Phys. Rev. B* **84**, 064118 (2011).
- [20] X. Zhong, H. Wang, J. Zhang, H. Liu, S. Zhang, H.-F. Song, G. Yang, L. Zhang, and Y. Ma, *Phys. Rev. Lett.* **116**, 057002 (2016).
- [21] H. Wang, X. Li, G. Gao, Y. Li, and Y. Ma, *Wiley Interdiscip. Rev.: Comput. Mol. Sci.* **8**, e1330 (2018).
- [22] T. Muramatsu, W. K. Wanene, M. Somayazulu, E. Vinitsky, D. Chandra, T. A. Strobel, V. V. Struzhkin, and R. J. Hemley, *J. Phys. Chem. C* **119**, 18007 (2015).
- [23] M. Rahm, R. Hoffmann, and N. Ashcroft, *J. Am. Chem. Soc.* **139**, 8740 (2017).
- [24] S. Zhang, L. Zhu, H. Liu, and G. Yang, *Inorg. Chem.* **55**, 11434 (2016).
- [25] C. Kokail, W. von der Linden, and L. Boeri, *Phys. Rev. Mater.* **1**, 074803 (2017).
- [26] Y. Ma, D. Duan, Z. Shao, H. Yu, H. Liu, F. Tian, X. Huang, D. Li, B. Liu, and T. Cui, *Phys. Rev. B* **96**, 144518 (2017).
- [27] Y. Ma, D. Duan, Z. Shao, D. Li, L. Wang, H. Yu, F. Tian, H. Xie, B. Liu, and T. Cui, *Phys. Chem. Chem. Phys.* **19**, 27406 (2017).
- [28] B. Liu, W. Cui, J. Shi, L. Zhu, J. Chen, S. Lin, R. Su, J. Ma, K. Yang, M. Xu *et al.*, *Phys. Rev. B* **98**, 174101 (2018).
- [29] K. Nagao, S. A. Bonev, A. Bergara, and N. W. Ashcroft, *Phys. Rev. Lett.* **90**, 035501 (2003).
- [30] Y. Wang, J. Lv, L. Zhu, and Y. Ma, *Phys. Rev. B* **82**, 094116 (2010).
- [31] Y. Wang, J. Lv, L. Zhu, and Y. Ma, *Comput. Phys. Commun.* **183**, 2063 (2012).
- [32] J. Lv, Y. Wang, L. Zhu, and Y. Ma, *Phys. Rev. Lett.* **106**, 015503 (2011).
- [33] L. Zhu, H. Liu, C. J. Pickard, G. Zou, and Y. Ma, *Nat. Chem.* **6**, 644 (2014).
- [34] J. P. Perdew, J. A. Chevary, S. H. Vosko, K. A. Jackson, M. R. Pederson, D. J. Singh, and C. Fiolhais, *Phys. Rev. B* **46**, 6671 (1992).
- [35] G. Kresse and J. Furthmüller, *Phys. Rev. B* **54**, 11169 (1996).
- [36] H. J. Monkhorst and J. D. Pack, *Phys. Rev. B* **13**, 5188 (1976).
- [37] P. Giannozzi, S. Baroni, N. Bonini, M. Calandra, R. Car, C. Cavazzoni, D. Ceresoli, G. L. Chiarotti, M. Cococcioni, I. Dabo *et al.*, *J. Phys.: Condens. Matter* **21**, 395502 (2009).
- [38] See Supplemental Material at <http://link.aps.org/supplemental/10.1103/PhysRevB.100.184502> for predicted structures at lower pressure, the internal energies (U), and the product of pressure and volume (PV) contributions to the enthalpy of $P4_2/mmc$ YSH₆ and $Cmcm$ LaSH₆, the calculated electronic band structure for lower-pressure structures, the comparison of total DOS between different hydrides, the origin of instability for $P4_2/mmc$ YSH₆ and $Cmcm$ LaSH₆ at low pressure, superconductivity of the $P4_2/mmc$ YSH₆ and $Cmcm$ LaSH₆ at 300 GPa, dynamical properties of predicted structures, and the separate contributions of nonhydrogen elements and hydrogen to the parameters determining T_c and structural information.
- [39] C. J. Pickard and R. J. Needs, *Nat. Phys.* **3**, 473 (2007).
- [40] M. I. McMahan and R. J. Nelmes, *Chem. Soc. Rev.* **35**, 943 (2006).
- [41] Y. Ma and J. S. Tse, *Solid State Commun.* **143**, 161 (2007).
- [42] A. D. Becke and K. E. Edgecombe, *J. Chem. Phys.* **92**, 5397 (1990).
- [43] A. Savin, O. Jepsen, J. Flad, O. K. Andersen, H. Preuss, and H. G. von Schnering, *Angew. Chem. Int. Ed.* **31**, 187 (1992).
- [44] R. Bader, *Atoms in Molecules: A Quantum Theory* (Oxford University Press, Oxford, 1994).
- [45] E. Zurek, R. Hoffmann, N. W. Ashcroft, A. R. Oganov, and A. O. Lyakhov, *Proc. Natl. Acad. Sci. USA* **106**, 17640 (2009).
- [46] T. Bi, N. Zarifi, T. Terpstra, and E. Zurek, *Reference Module in Chemistry, Molecular Sciences and Chemical Engineering* (Elsevier, Amsterdam, 2019).
- [47] A. Shamp and E. Zurek, *Nov. Supercond. Mater.* **3**, 14 (2017).
- [48] L. Zhang, Y. Wang, J. Lv, and Y. Ma, *Nat. Rev. Mater.* **2**, 17005 (2017).
- [49] Y. Quan and W. E. Pickett, *Phys. Rev. B* **93**, 104526 (2016).
- [50] L. Liu, C. Wang, S. Yi, K. W. Kim, J. Kim, and J.-H. Cho, *Phys. Rev. B* **99**, 140501(R) (2019).
- [51] J. A. Flores-Livas, L. Boeri, A. Sanna, G. Profeta, R. Arita, and M. Eremets, [arXiv:1905.06693](https://arxiv.org/abs/1905.06693).
- [52] P. B. Allen and R. C. Dynes, *Phys. Rev. B* **12**, 905 (1975).
- [53] D. Papaconstantopoulos, B. M. Klein, M. Mehl, and W. Pickett, *Phys. Rev. B* **91**, 184511 (2015).
- [54] Y. Quan, S. S. Ghosh, and W. E. Pickett, [arXiv:1906.02695](https://arxiv.org/abs/1906.02695).
- [55] J. J. Hopfield, *Phys. Rev.* **186**, 443 (1969).
- [56] W. Weber, *Phys. Rev. B* **8**, 5093 (1973).